

# Projection of wildfire activity in southern California in the mid-twenty-first century

Xu Yue · Loretta J. Mickley · Jennifer A. Logan

Received: 24 June 2013 / Accepted: 9 December 2013 / Published online: 21 December 2013  
© Springer-Verlag Berlin Heidelberg 2013

**Abstract** We estimate area burned in southern California at mid-century (2046–2065) for the Intergovernmental Panel on Climate Change A1B scenario. We develop both regressions and a parameterization to predict area burned in three ecoregions, and apply present-day (1981–2000) and future meteorology from the suite of general circulation models to these fire prediction tools. The regressions account for the impacts of both current and antecedent meteorological factors on wildfire activity and explain 40–46 % of the variance in area burned during 1980–2009. The parameterization yields area burned as a function of temperature, precipitation, and relative humidity, and includes the impact of Santa Ana wind and other geographical factors on wildfires. It explains 38 % of the variance in area burned over southern California as a whole, and 64 % of the variance in southwestern California. The parameterization also captures the seasonality of wildfires in three ecoregions of southern California. Using the regressions, we find that area burned likely doubles in Southwestern California by midcentury, and increases by 35 % in the Sierra Nevada and 10 % in central western California. The parameterization suggests a likely increase

of 40 % in area burned in southwestern California and 50 % in the Sierra Nevada by midcentury. It also predicts a longer fire season in southwestern California due to warmer and drier conditions on Santa Ana days in November. Our method provides robust estimates of area burned at mid-century, a key metric which can be used to calculate the fire-related effects on air quality, human health, and the associated costs.

**Keywords** Wildfire · Ensemble projection · Southern California · Santa Ana wind

## 1 Introduction

Fires burned  $\sim 25,000$  km<sup>2</sup> in California in the past decade, an area almost 10 times that of the Yosemite National Park. Large fires cause tremendous economic loss (<http://www.ncdc.noaa.gov/billions/>) and threaten lives, especially in southern California. Emissions from wildfires significantly worsen air quality in local and downwind regions and adversely affect human health (Mott et al. 2002; Hlavka et al. 2005; Kunzli et al. 2006; Pfister et al. 2008). Projection of future wildfire activity in southern California is challenging, not only because fires in this area are influenced by a mix of factors including human activity, fuel load, topography, and weather conditions (Syphard et al. 2008; Peterson et al. 2011), but also because the projected changes in meteorology in this region are very uncertain (Christensen et al. 2007). In this study, we project future area burned in southern California at midcentury (2046–2065). We examine the factors contributing to area burned, and we develop two fire tools, parameterization and regressions, to predict future area burned with meteorological variables from a suite of general circulation models (GCMs). Since area burned is required for

---

**Electronic supplementary material** The online version of this article (doi:10.1007/s00382-013-2022-3) contains supplementary material, which is available to authorized users.

---

X. Yue · L. J. Mickley · J. A. Logan  
School of Engineering and Applied Sciences,  
Harvard University, Cambridge, MA, USA

*Present Address:*

X. Yue (✉)  
School of Forestry and Environmental Studies,  
Yale University, New Haven, CT, USA  
e-mail: xuyeseas@gmail.com

calculation of fire emissions, our work represents the first step toward estimating the environmental and health impacts of wildfires in coming decades in this highly populated region.

As a populous and mountainous state, California has a unique set of geographic and meteorological parameters associated with wildfires. Human activity has both positive and negative influences on wildfires in California (Syphard et al. 2007). People cause most fires in the state, and ignitions are usually close to roads, trails, and populated areas (Syphard et al. 2008). However, fires in the state are more likely to spread when they are far from urban areas in regions where fire suppression is not practiced (Syphard et al. 2008). In addition, the rugged terrain of remote regions makes access for firefighters difficult, while the high fuel load in these regions increases fire severity. These last two factors contribute to large area burned in remote regions (Keeley et al. 2009).

Most of the extremely large wildfires in southern California are associated with Santa Ana winds, strong offshore winds characterized by low humidity (Schroeder et al. 1964; Moritz 1997; Keeley et al. 2009). These winds develop as a consequence of a steep pressure gradient between the Great Basin and the Los Angeles area (Raphael 2003) and are strengthened as they channel through the complex local topography (Jones et al. 2010). The Santa Ana winds occur most frequently in winter but have their greatest impact on wildfires in autumn, when air temperatures are still high and vegetation has dried out during the preceding summer (Westerling et al. 2004; Keeley et al. 2009). Fire models that consider the impact of Santa Anas significantly increase the predicted area burned (Peterson et al. 2011), but the modeled fire-Santa Ana relationship has not been well validated.

Projections of future wildfire activity in southern California under global warming scenarios are few and they show contradictory results. Westerling and Bryant (2008) developed a statistical model for large fires in California by taking into account the impacts of climate and topography. Using simulated meteorological variables from two GCMs, they predicted that the probability of large fires in southern California will decrease by 29 % by 2100 using one GCM but increase by 28 % with the other. Lenihan et al. (2008) used the same GCM output to drive a dynamic global vegetation model (DGVM) and found that the annual area burned decreases more than 40 % along the southern coast of California for one GCM but increases more than 50 % for another by 2100, a result similar to Westerling and Bryant (2008) but for the opposite GCMs. Westerling et al. (2011) applied an approach similar to that in Westerling and Bryant (2008) using output from 3 GCMs for 2 climate scenarios. They calculated median increases of 20–40 % in area burned for California by 2085, but the 3 GCMs

predicted opposing changes in area burned in the south of the state. These studies used different fire schemes and relied on the output from only 1–3 GCMs, which may explain the inconclusive results. They also did not account for the effects of the Santa Ana winds. The prediction of Santa Anas in a future atmosphere is uncertain, as different trends are projected depending on the climate model, scenario, and the criteria used to identify Santa Ana events (Miller and Schlegel 2006; Hughes et al. 2011).

In an earlier study, we projected future wildfire activity in the western US using two fire prediction schemes and output from 15 climate models (Yue et al. 2013, hereinafter referred to as Y2013). We developed fire models by regressing meteorological variables and fire indexes onto observed area burned in each of six ecoregions with a stepwise approach. We also developed a parameterization that calculates daily area burned as a function of temperature, relative humidity, and precipitation in each grid. Both approaches performed well in forested regions but poorly in southern California, even when we took into account the impact of antecedent meteorological conditions as suggested by some studies (e.g., Westerling et al. 2003; Littell et al. 2009).

In this study, we build on the multi-model prediction approach in Y2013 and project future area burned in southern California with updated fire prediction schemes. First, we divide the original area into three sub-regions and use meteorological data with higher spatial resolution. Second, we consider the influence of elevation, population, and fuel load on wildfire activity. Third, we take into account the impacts of Santa Ana winds to improve our fire prediction tools. Our work is the first to validate the modeled relationship between fires and Santa Ana winds and apply it to simulated climate from multiple GCMs. In Sect. 2, we describe the data we use, and in Sect. 3 we develop and evaluate fire models for the present-day area burned. We show the projections of future area burned in Sect. 4 and discuss these results in the final section.

## 2 Data

### 2.1 Fire data

We use the interagency fire report data managed by the National Wildfire Coordinating Group from the Fire and Aviation Management Web Applications (FAMWEB, <http://fam.nwcg.gov/fam-web/weatherfirecd/>, downloaded on March 25th, 2011). The data are collected by five agencies: the US Forest Service (USFS), Bureau of Land Management (BLM), Bureau of Indian Affairs (BIA), Fish and Wildlife Service (FWS), and National Park Service (NPS). Each report gives the name, location (longitude and

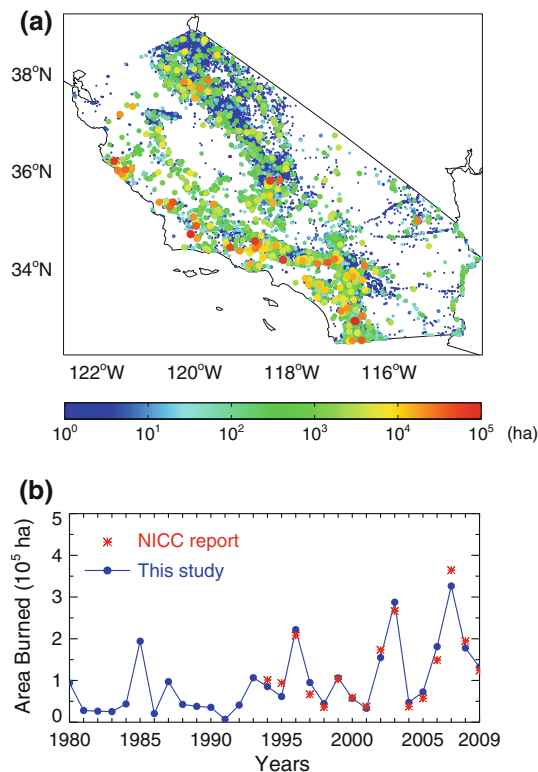


**Fig. 1** **a** Incidence of fires in southern California during 1980–2009. Both the relative size and the color of each point indicate the area of fire. **b** Annual total area burned in southern California during 1980–2009. The red stars represent results from the NICC annual reports, and the blue points are derived in this study from FAMWEB

latitude), time (start and end), ignition source (lightning or human) and area burned of an individual fire. Although the USFS provides fire reports back to 1914, more than 90 % of the records are for fires after 1980. The quality of pre-1980 data is uncertain (Westerling et al. 2003), so we select fires in 1980–2009. The same fire sometimes burns in land managed by different agencies, so we filter the data for two or more records reporting fires with the same name and area burned that occur within 50 km of each other on the same day. We compile fire records only for southern California, which we define to be south of the line linking Lake Tahoe and San Francisco (Fig. 1a). All the fires in the same month are aggregated into a  $0.5^\circ \times 0.5^\circ$  grid.

We also use the annual fire reports from the National Interagency Coordination Center (NICC, <http://www.nifc.gov/nicc/>). The NICC manages fire reports from federal agencies, states, and privately owned land, and as a result has more complete datasets relative to the FAMWEB. However, it provides only the annual total number and area of fires back to 1994 in each of the 11 pre-defined geographic areas in the United States. The domain of southern California defined in our study is consistent with that in the NICC, so we use the latter as a check on our compilation from the FAMWEB.

## 2.2 Geographic data

We obtain the topographic data ETOPO from the NOAA National Geographic Data Center (<http://www.ngdc.noaa.gov/>). It gives global topography with a resolution as high as 2 min ( $\sim 3$  km). We download the gridded 1 km population map for the United States for 2000 from the NOAA National Climatic Data Center (<http://www.ncdc.noaa.gov/>). We use the fuel load database of the USFS, the Fuel Characteristic Classification System (FCCS, <http://www.fs.fed.us/pnw/fera/fccs/>, downloaded on May 12th, 2011) (McKenzie et al. 2007; Ottmar et al. 2007). The 1 km  $\times$  1 km fuelbed map for the US is derived from the distribution of vegetation types from the Landscape Fire and Resource Management Planning Tools (LANDFIRE, <http://www.landfire.gov/>). We group the FCCS fuel categories into seven fuel types, including litter and light fuels, medium fuels, heavy fuels, duff, grass, shrub, and canopy, as in Spracklen et al. (2009). We use shrub load as a variable to estimate fire distribution because we obtain a statistically significant relationship between fire probability and shrub load. We aggregate population and fuel load data onto the  $2' \times 2'$  grid of the topographic data.

## 2.3 Meteorological data

For the regressions, we use daily measurements at 361 FAMWEB weather sites in southern California, including local noon temperature and relative humidity (*RH*) at 2 meters above ground level (AGL), wind speed and direction at 10 m AGL, as well as the daily total precipitation. These variables are applied directly in the regressions, and are used to calculate the fire indexes described below. An earlier version of the FAMWEB weather data was used in Spracklen et al. (2009). Y2013 relied on the daily meteorological dataset from the Global Surface Summary of the Day (GSOD), which at that time had somewhat better temporal and spatial continuity than FAMWEB in the western United States. However, the FAMWEB dataset has recently been updated and is now more complete, with only 1–3 % of the days missing. We do not use the GSOD dataset here as it has fewer sites in southern California than FAMWEB, and it does not include wind direction, essential for definition of the Santa Ana winds.

We use daily gridded data from the North American Regional Reanalysis (NARR, Mesinger et al. 2006) as input for the parameterization. The daily NARR reanalyses provide diurnally averaged meteorological fields, including temperature and *RH* at 2 m AGL, precipitation, and sea level pressure (*SLP*), with a resolution of 32 km. We aggregate the data onto a  $0.5^\circ \times 0.5^\circ$  grid. We do not use the NARR for the regressions since the reanalysis underestimates wind speeds by  $\sim 60$  % in southern California on

high wind days (Hughes and Hall 2010). The 32-km resolution is not fine enough to resolve the local complex terrain, and as a result cannot capture the Santa Ana winds. We compare the differences between FAMWEB and NARR meteorology in section A of the supplemental information.

#### 2.4 Fire weather indexes

Following Flannigan et al. (2005), we use the fire indexes from the Canadian Fire Weather Index system (CFWIS) as predictors in the regression models (Van Wagner 1987). The CFWIS consists of seven components, including three fuel moisture codes and four fire behavior indexes (Table S1). The fuel moisture codes indicate the moisture content in different kinds of fuels, such as Fine Fuel Moisture Code (FFMC) for litter/fine fuels, Duff Moisture Code (DMC) for moderate duff/woody materials, and Drought Code (DC) for heavy forest fuels. The Initial Spread Index (ISI), Build-up Index (BUI), and Fire Weather Index (FWI) describe fire behaviors, including the rate of fire spread, fuel availability, and fire intensity. The Daily Severity Rating (DSR) is calculated as an exponential function of the FWI to reflect the difficulty in controlling fires and is a strong function of wind speed.

We use the daily meteorological data from FAMWEB to calculate CFWIS indexes. We first divide southern California into three ecoregions based on Hickman (1993) (Fig. 2a). Fires in these regions account for 94 % of the total area burned, and we assume that similar fuel types, weather conditions, and fire behaviors occur in each ecoregion. We calculate the daily average meteorological fields for each ecoregion by aggregating the observations from the sites located therein. Temperatures and *RH* at each site are adjusted for elevation so that they represent weather conditions at the average height of the ecoregion.

#### 2.5 CMIP3 model archives

We use the meteorological output of 14 GCMs from the World Climate Research Programme's (WCRP) Coupled Model Intercomparison Project phase 3 (CMIP3) multi-model dataset (Meehl et al. 2007) (Table 1), including daily mean and maximum surface temperature, wind speed, *SLP*, and total precipitation. CMIP3 does not specify the height AGL of the modeled surface variables, but we account for possible discrepancies with observations through bias-correction (Sect. 4). Daily surface *RH* is not provided by CMIP3, so we calculate that variable as the ratio of specific humidity to saturated humidity. We calculate surface specific humidity at the grid level by extrapolating from the value at the lowest model level, while saturated humidity is derived from surface

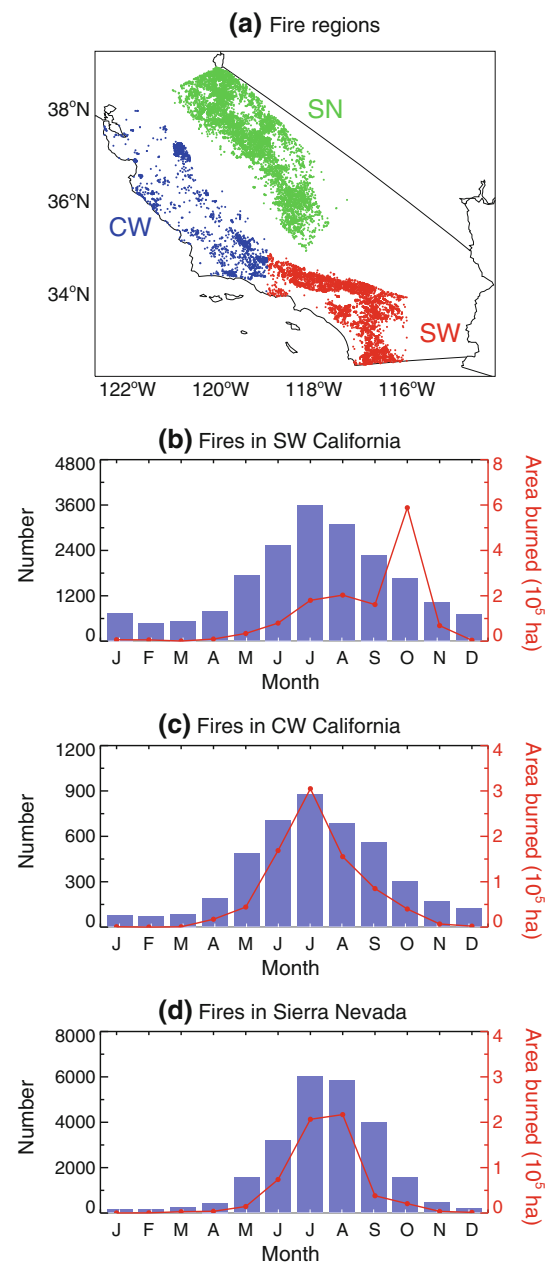


**Fig. 2** a Spatial distribution of three fire regions examined in this study: southwestern California (SW); central western California (CW); and the Sierra Nevada (SN). b–d Seasonality of total fire numbers (purple bars) and total area burned (red lines) in these regions summed over the period 1980–2009

temperature and pressure. The output is interpolated onto the  $0.5^\circ \times 0.5^\circ$  grid. We acknowledge that our approach may not resolve the impacts of topography on meteorological variables as well as statistically downscaled GCM data might. However, the downscaled GCM datasets either lack important fire-weather variables like *RH* and wind velocity (e.g., the Bias Corrected and Downscaled WCRP CMIP3 Climate Projections, <http://gdo-dcp.ucllnl.org/>), or use only a subset of the CMIP3 GCMs and so may be

**Table 1** List of models whose output is utilized in the fire projections for southern California

Model name	Resolution	Country
CCCMA-CGCM3.1 (T47)	3.75° × 3.75°	Canada
CCCMA-CGCM3.1 (T63)	2.8125° × 2.8125°	Canada
CNRM-CM3	2.8125° × 2.8125°	France
CSIRO-MK3.0	1.875° × 1.875°	Australia
CSIRO-MK3.5	1.875° × 1.875°	Australia
GFDL-CM2.0	2.5° × 2.0°	USA
GFDL-CM2.1	2.5° × 2.0°	USA
GISS-AOM	4.0° × 3.0°	USA
IAP-FGOALS1.0	2.8125° × 3.0°	China
INGV-ECHAM4	1.125° × 1.125°	Italy
IPSL-CM4	3.75° × 2.5°	France
MIUB-ECHOG	3.75° × 3.75°	Germany
MPI-ECHAM5	1.875° × 1.875°	Germany
MRI-CGCM2.3.2	2.8125° × 2.8125°	Japan

Three-dimensional fields from the models are provided at the same fixed vertical levels for all models

biased for the ensemble projection (e.g., the North American Regional Climate Change Assessment Program, <http://www.narccap.ucar.edu/>).

For the present-day simulation (1981–2000), we use output from the 20C3M scenario, which includes the observed trends of greenhouse gases in the twentieth century. For the future (2046–2065), we use output from the IPCC A1B scenario, which describes a world with moderate growth in fossil fuel emissions in the first half of the twenty-first century but a gradual decrease after 2050. The CO<sub>2</sub> concentration in this scenario reaches 522 ppm by midcentury, a similar level as that for the A2 scenario, which assumes no special actions to control CO<sub>2</sub> emissions during the twenty-first century (Solomon et al. 2007). To remove the systematic biases in individual models, we use long-term mean present-day (1980–2009) observations to bias-correct the model output in both the 20C3M and the A1B scenarios, as discussed in Sect. 4. We estimate the significance level of the changes in meteorological variables, Santa Ana winds, and area burned using a Student's *t* test. We consider a change is significant if  $p < 0.05$ , unless otherwise stated.

### 3 Simulation of present-day area burned

#### 3.1 Relationship of fires and weather in southern California

Figure 1a shows the more than 55,000 fire incidents during 1980–2009. Most fires occur on mountains within

~120 km of the coastline or in the Sierra Nevada. Fires in other parts of the state are scarce because of limited fuel load or constraints from agriculture. The human impact is made clear by the large number of fires along highways, as indicated by the strings of blue dots radiating eastward from southern California, and along the Colorado River, indicated by the green dots at the border of California and Arizona. Human ignitions accounted for more than 90 % of wildfire incidents in southern California in 2000–2009 according to NICC reports, but meteorological conditions strongly influence the size and interannual variability of fires in this region (Schroeder et al. 1964; Westerling et al. 2004). Figure 1b shows the large interannual variability in area burned, with large fires in 1985, 1996, 2003, and 2007 contributing more than 35 % of the total area burned during 1980–2009. Comparison of the FAMWEB annual area burned with the values from the NICC reports shows that our compilation is reasonable ( $r = 0.98$ , Fig. 1b).

We focus on three ecoregions in southern California (Fig. 2a). Two, southwestern (SW) California and central western (CW) California, are located along the coast, where shrub and grass provide the dominant fuels. Fires in CW California occur closer to the ocean than in SW California, where urban areas line the coast. Large fires in SW California are usually associated with the Santa Ana winds. The third ecoregion, the Sierra Nevada, is a forested mountainous area (elevation >1,500 m). There are fewer large fires in this region (Fig. 1a).

The number of wildfires peaks in summer, with a maximum in July, in all regions (Figs. 2b–d), as does area burned in CW California and the Sierra Nevada. However, in SW California, area burned peaks in October due to extremely large fires in 2003 and 2007, and area burned is largest here. The highest temperatures and the lowest precipitation rates occur in summer in all three ecoregions (Fig. S1), consistent with the maximum in area burned in CW California and the Sierra Nevada. The peak values of area burned in October in SW California are associated with the Santa Ana winds and the still warm and dry weather conditions of mid-autumn (Keeley et al. 2009).

#### 3.2 Fire regressions

We develop relationships between the observed area burned and FAMWEB meteorological variables and fire indexes, using a stepwise regression method in each ecoregion. The method was first used by Flannigan et al. (2005) to project future area burned in Canada under a scenario with tripled CO<sub>2</sub>. Spracklen et al. (2009) applied a similar method to project future area burned over the western United States by the midcentury. Y2013 improved on the approach of Spracklen et al. (2009) by adding an independence test for selected terms, which checks for

**Table 2** Regression models for each ecoregion in southern California

Ecoregion	Regression model <sup>a</sup>	R <sup>2</sup> (%) <sup>b</sup>
SW California	$3.0 \times 10^4 \text{ T.FS} + 1.1 \times 10^2 \text{ DMC}_{\max}(-2) - 9.4 \times 10^5 \text{ DSR}_{\max} + 1.2 \times 10^3 \text{ RH.ANN} - 1.6 \times 10^2 \text{ DC}(-2) + 4.0 \times 10^5$	46
CW California	$-5.5 \times 10^3 \text{ T.FS} + 1.1 \times 10^2 \text{ DMC}_{\max}(-2) - 9.4 \times 10^5 \text{ DSR}_{\max} + 1.2 \times 10^3 \text{ RH.ANN} - 1.6 \times 10^2 \text{ DC}(-2) + 4.0 \times 10^5$	40
Sierra Nevada	$-6.2 \times 10^3 \text{ T.FS} + 1.1 \times 10^2 \text{ DMC}_{\max}(-2) - 9.4 \times 10^5 \text{ DSR}_{\max} + 1.2 \times 10^3 \text{ RH.ANN} - 1.6 \times 10^2 \text{ DC}(-2) + 4.0 \times 10^5$	43

<sup>a</sup> T.FS: mean temperature during fire season;  $\text{DMC}_{\max}(-2)$ : maximum Duff Moisture Code during the fire season 2 years before;  $\text{DSR}_{\max}$ : maximum Daily Severity Rating index during fire season; RH.ANN: annual mean relative humidity;  $\text{DC}(-2)$ : average Drought Code during the fire season 2 years before;  $\text{T}_{\max}.\text{AUT}(-2)$ : autumn mean daily maximum temperature 2 years before; T.FS: mean temperature during fire season

<sup>b</sup> R<sup>2</sup> represents the percentage of variance in area burned explained by the regression

correlation among potential predictors. In addition, Y2013 took into account the impact of antecedent weather factors on the current area burned, as suggested by Westerling et al. (2003) and Littell et al. (2009). We follow the same steps as Y2013 and develop regression models for area burned during the fire season (May–October) in the three ecoregions.

We derive monthly meteorological fields for mean temperature, daily maximum temperature, precipitation, and *RH* from the FAMWEB daily observations. These variables are aggregated to calculate seasonal (spring, summer, autumn, and winter), annual, and fire-season averages in each ecoregion. The seven daily CFWIS indexes are used to calculate mean and maximum values during the fire season. These steps give 38 factors for the current year. Including these factors from the previous 1–2 years gives 114 potential predictors for the stepwise regression in each ecoregion.

Table 2 shows that both current and antecedent factors are selected in the regressions. Current meteorological factors dominate the fire-weather relationships in SW and CW California, with larger area burned when temperature is higher or *RH* is lower. However, weather conditions in previous years play the dominant role in the Sierra Nevada, where the area burned is anti-correlated with the autumn mean maximum temperature 2 years earlier. The reasons for this relationship are not clear, but may involve greater soil moisture content being maintained at cooler temperatures (Wu and Dickinson 2004), which enhances vegetation growth in the following growing season. Figure 3 compares annual observed and modeled area burned for 1980–2009 for each ecoregion. The regressions explain 40–46 % of the variance in area burned for three ecoregions and 59 % for the whole of southern California, a

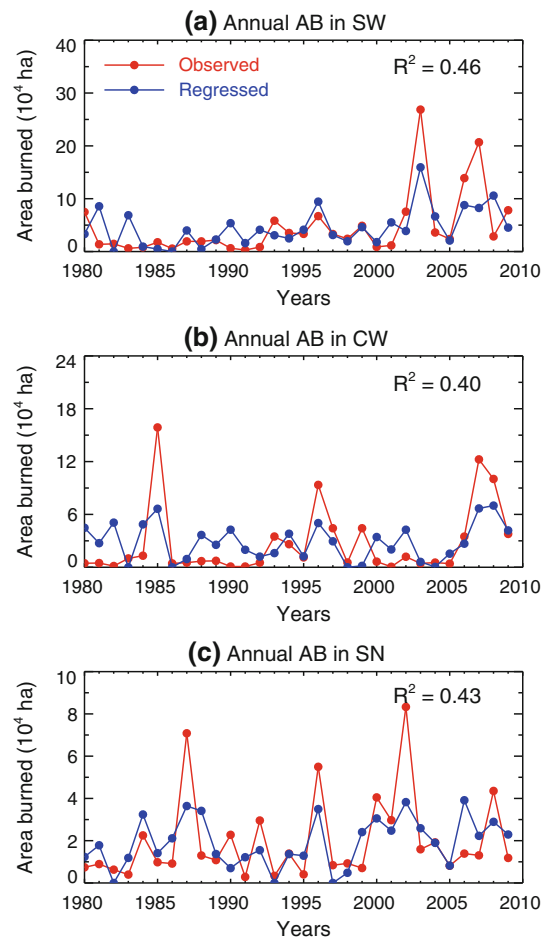


**Fig. 3** Time series of observed (red) and modeled (blue) total annual area burned in three ecoregions of Southern California during 1980–2009. Modeled area burned is calculated with stepwise linear regressions. Negative values are set to zero. The correlation *r* between the observed and calculated area burned is shown in the right-upper corner of each figure. All the correlations are significant at  $p < 0.001$ . Acronyms for the ecoregions are defined in Fig. 2

large improvement on our result in Y2013, which yielded R<sup>2</sup> of only 0.25 for the entire region. The success of the new regression in SW California derives in part from the high quality of the FAMWEB data, which captures strong wind events like the Santa Ana, and in part from inclusion of the fire index DSR in the regression fit, which describes the impact of strong winds on the spread rate of fires.

### 3.3 Fire parameterization model

In Y2013 we parameterized daily area burned over the western United States as a function of temperature, *RH*, and precipitation. We improve this approach for area burned in southern California by taking into account the impacts of elevation, population, and fuel load on the fire probability, and the influence of the Santa Ana winds on the fire size.

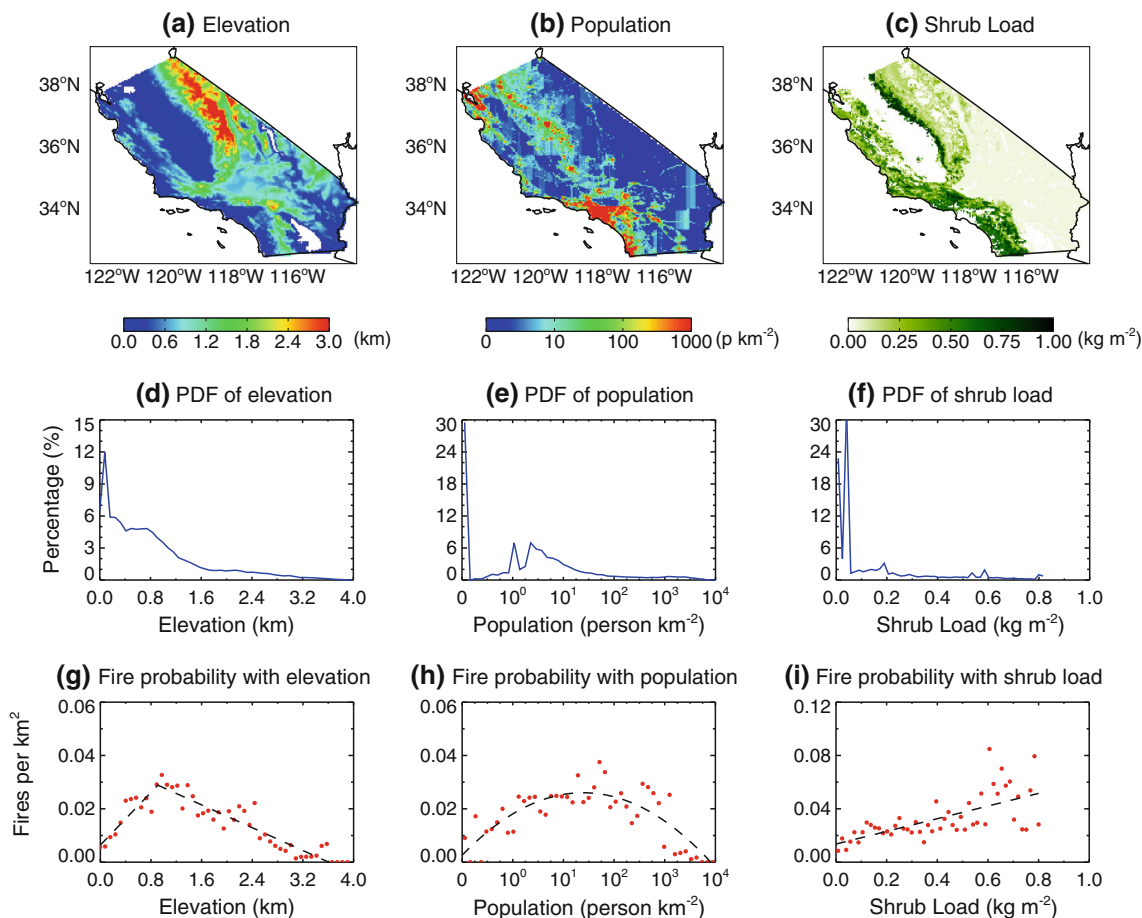


**Fig. 4** Spatial distributions of **a** elevation, **b** population, and **c** shrub fuel load in southern California. **d–f** Show the observed probability density functions (PDF) of these variables. The probability of fires associated with these factors is shown in **(g–i)**. For these panels we first binned the observed number of fires per square kilometer during

1980–2009 by small, equal-sized increments across the range of each factor. The red points in panels **(g–i)** represent the average number of fires per square kilometer in each increment for this time period. The *dark dashed lines* are calculated with Eqs. (1)–(3) and represent an empirical fit to the fire probability data

### 3.3.1 Parameterization of fire probability

Fire probability quantifies the likelihood for a fire to occur in a specific area during a specific period. It depends on the sources of ignition, availability of fuel, and the combustibility of the fuel (Schoennagel et al. 2004). These factors are associated with the geographic characteristics of fire locations, such as topography, population, and fuel load (Syphard et al. 2008; Preisler et al. 2011). In southern California there are mountains in the north, plains in the center, and hills near the coast (Fig. 4a). One-fourth of the region has elevation lower than 200 m, while nearly a third is higher than 1 km (Fig. 4d). Fire probability was  $\sim 0.03$  fires  $\text{km}^{-2}$  in areas with elevations of 900–1,400 m, and less at lower and higher altitudes in 1980–2009 (Fig. 4g). Population density is highest in the Central Valley and coastal regions, with few inhabitants in the mountains (Fig. 4b). The probability of fires was almost constant for areas with a population density of 1–1,000  $\text{km}^{-2}$ , but

tended toward zero beyond this range (Fig. 4h). The fuel load of shrub vegetation (Fig. 4c) has a similar distribution to that of fire locations (Fig. 1a). Fire probability showed a linear relationship with the fuel load (Fig. 4i).

Based on the relationships in Fig. 4g–i, we used least-square regression to determine fire probability as functions of elevation ( $z$ , km), population ( $p$ , persons  $\text{km}^{-2}$ ), and fuel load ( $f$ ,  $\text{kg m}^{-2}$ ):

$$f_1(z) = \begin{cases} 0.0247z + 0.006 & 0 \leq z < 0.9 \\ -0.0107z + 0.039 & 0.9 \leq z < 3.6 \end{cases} \quad (1)$$

$$f_2(p) = -0.004 \log_{10}^2(p + 0.1) + 0.011 \log_{10}(p + 0.1) + 0.018 \quad (2)$$

$$f_3(f) = 0.0475f + 0.0136 \quad (3)$$

Any negative values predicted with Eqs. (1)–(3) are set to zero. Fire probability considering all factors is calculated as  $FP(x, y) = f_1[z(x,y)] \times f_2[p(x,y)] \times f_3[f(x,y)]$ , where  $x$  and  $y$  are longitude and latitude. We normalize by

dividing by the maximum value of  $FP(x, y)$  for all of southern California to estimate the relative fire probability. Figure 5a shows the predicted normalized values of  $FP(x, y)$  for 1980–2009 on the  $2' \times 2'$  grid. The distribution of relative fire probabilities compares well with the observed incidence of fires, with maxima along the west coast and in the mountains (Fig. 1a). We interpolate the relative fire probability onto a  $0.5^\circ \times 0.5^\circ$  grid for the fire parameterization (Fig. 5b).

### 3.3.2 Santa Ana winds and area burned

Santa Ana winds are strong and extremely dry offshore winds that periodically blow across southern California. They occur most frequently in winter, but also in autumn, when they are strongly associated with fire weather conditions (Schroeder et al. 1964). The Santa Ana winds result from a combination of the large-scale circulation and the complex local topography, as shown by Conil and Hall (2006) who downscaled observed winds to 6 km resolution in their analysis. The NARR, with resolution of 32 km, significantly underestimates the Santa Ana wind speeds (Hughes and Hall 2010). Since we use relatively coarse resolution GCM output to predict future fires, we need to parameterize the effects of Santa Ana winds using relevant features of the large-scale circulation, which most climate models can simulate successfully.

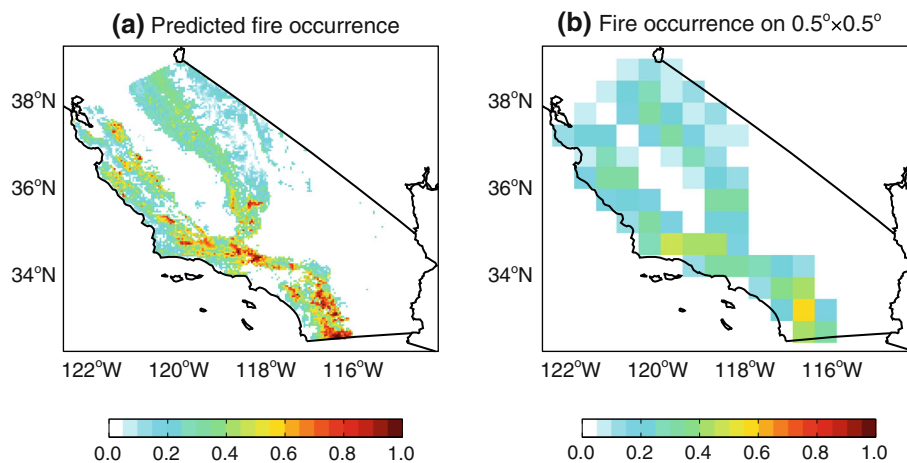
Observations indicate a link between Santa Ana winds and the large-scale pressure gradient between the Great Basin and the Los Angeles area (Raphael 2003). The strong winds are heated and dried as they descend from the deserts at high elevations to the low-level coastal region in southern California, resulting in low  $RH$  and strong cold air advection east of Los Angeles (Conil and Hall 2006). Many studies used  $SLP$  gradient to diagnose the wind (e.g., Raphael 2003; Jones et al. 2010). However, Hughes and Hall (2010) suggested that the cold air advection, rather

than the large-scale pressure gradient, is the dominant driver for Santa Ana variability. In a recent study, Abatzoglou et al. (2013) successfully predicted Santa Ana activity by constructing a two-parameter threshold model with both the  $SLP$  gradient and 850 hPa temperature advection. However, calculation of daily average temperature advection requires sub-daily wind speed and temperature, which are not available for most CMIP3 GCMs. Since cold air advection is not available in the CMIP3 archive,  $SLP$  gradient and  $RH$  are likely the best available large scale proxy for Santa Anas; for future work it would be interesting to see if the fire parameterization could be improved even more by inclusion of a more realistic representation of Santa Ana activity.

We investigate the pattern of anomalous  $SLP$  and  $RH$  in the NARR during the periods with strong winds, which we define as  $>4.5 \text{ m s}^{-1}$  averaged over the FAMWEB site data in SW California in October. Figure 6a–d demonstrate that strong winds are associated with moderately high pressures over the Great Basin and anomalously low  $RH$  along the west coast. Following the approach of Conil and Hall (2006), we divide strong wind days into offshore, onshore, and alongshore groups. Days with strong offshore winds, typical of Santa Ana winds, are associated with anomalously high  $SLP$  over the Great Basin, a strong positive gradient in  $SLP$  between the Great Basin and Los Angeles (Fig. 6b), and low  $RH$  in southern California (Fig. 6e). In contrast, extremely low pressure anomalies arise in the Great Basin on days with onshore winds (Fig. 6c) that bring moist air inland, increasing  $RH$  (Fig. 6f).

To quantify the relationship between Santa Ana winds and large-scale meteorology, we use the daily differences in  $SLP$  between the Great Basin and the Los Angeles region as defined by the boxes in Fig. 6b. The  $SLP$  difference is positive for 95 % of days with offshore winds in SW California in October, as shown in Fig. 7, and the

**Fig. 5** Predicted normalized fire probability in southern California as functions of elevation, population, and fuel load on a resolution of **a**  $2' \times 2'$  and **b**  $0.5^\circ \times 0.5^\circ$ . The probabilities are based on observed fire number during 1980–2009. Those regions with a probability of 1 have the greatest likelihood of fires, equivalent to 0.1 fires per square kilometer during the 30-year time period





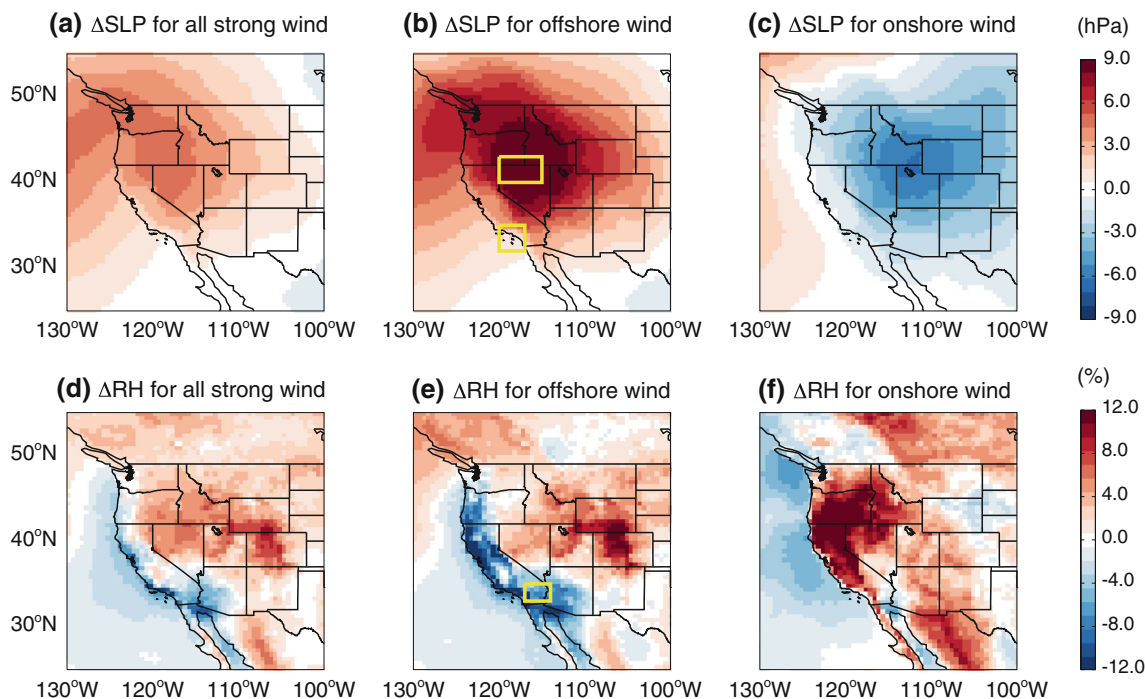


**Fig. 6** Distribution of observed anomalous daily mean (a) sea level pressure (*SLP*) and (d) surface relative humidity (*RH*) on those days when the average wind speed in Southwestern California is larger than  $4.5 \text{ m s}^{-1}$  in October. *SLP* and *RH* are from NARR reanalyses and wind speed and direction are from the FAMWEB sites. (b) and (e) are similar to (a) and (d) but show observations on days with strong, offshore winds. (c) and (f) are similar to (a) and (d) but for strong, onshore winds. An offshore wind day is defined when more than 50 % of the available meteorological sites report a wind angle of  $0^\circ\text{--}135^\circ$ ,

relative to North. An onshore wind is defined when more than 50 % of the available meteorological sites report a wind direction between  $180^\circ$  and  $315^\circ$ . The two yellow boxes in (b), the upper within the Great Basin ( $40\text{--}43^\circ\text{N}$ ,  $115\text{--}120^\circ\text{W}$ ) and the lower on Los Angeles ( $32\text{--}35^\circ\text{N}$ ,  $117\text{--}120^\circ\text{W}$ ), are used to calculate the pressure gradients in Figs. 7 and 9. The box in (e) contains San Diego ( $33\text{--}35^\circ\text{N}$ ,  $114\text{--}117^\circ\text{W}$ ), which is used to calculate relative humidity in the definition of Santa Anas

pressure gradient correlates with offshore wind speed with a significant correlation of  $r = 0.47$ . There is no significant relationship between the *SLP* gradient and wind speed for onshore or along shore winds. A similar relationship between offshore winds and the pressure gradient is found in November but not September (not shown).

Figures 6 and 7 suggest that local *RH* together with a strong *SLP* gradient can be used as indicators of Santa Ana winds. We select a *RH* box centered on San Diego, east of Los Angeles, because it is on the path of Santa Anas (Conil and Hall 2006; Hughes and Hall 2010). We do not select the extremely low *RH* along the coastal areas as an indicator, because climate models usually have difficulties simulating the steep *RH* gradient from the ocean to dry land. We find no significant correlation of *RH* as defined here with the *SLP* gradient between the Great Basin and Los Angeles: some days experience a strong *SLP* gradient but moist weather. By using a combination of the *SLP* gradient and *RH*, we better identify the dry, windy weather typical of Santa Anas. In an approach similar to ours, Abatzoglou et al. (2013) recently defined thresholds in *SLP* gradients and 850 hPa temperature advection as way to diagnose Santa Anas.

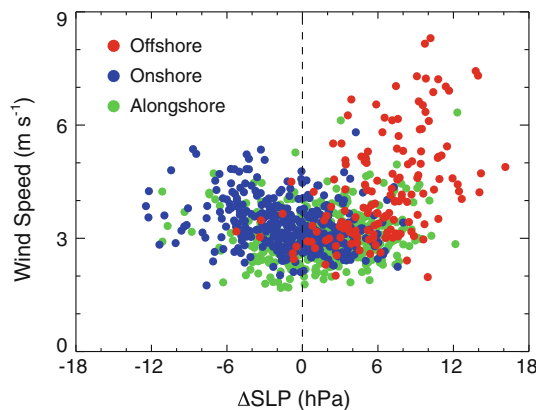


**Fig. 7** Average wind speed in Southwestern California and *SLP* difference between the two yellow boxes (upper minus lower) in Fig. 6b. Each point represents 1 day of October during 1980–2009. The red points indicate offshore winds, the blue points show onshore winds, and the green points show alongshore wind. The wind speed and wind direction are calculated with FAMWEB site observations and *SLP* is from NARR reanalyses

We define a day with Santa Ana winds if the daily *SLP* gradient exceeds 7.5 hPa and the *RH* is  $<30\%$  within a box in SW California (see Fig. 6e). The two threshold values were

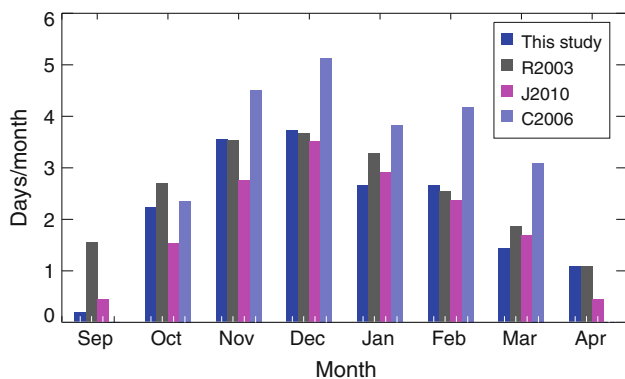


**Fig. 8** Seasonality of Santa Ana winds as defined by this study and as reported by others (R2003: Raphael 2003; J2010: Jones et al. 2010; C2006: Conil and Hall 2006). Each bar represents the average number of Santa Ana days per month over 1980–2009 (our study), 1968–2000 (Raphael 2003), 1979–2008 (Jones et al. 2010), and 1995–2003 (Conil and Hall 2006). Our results exhibit root-mean-square errors of 0.57 day with Raphael (2003), 0.48 day with Jones et al. (2010), and 1.15 day with Conil and Hall (2006)

selected by trial-and-error so that the seasonality of the Santa Ana winds predicted using *SLP* and *RH* from the NARR matches that reported by previous studies (Fig. 8). These studies used different definitions of Santa Ana events and relied on different meteorological datasets. Figure 8 shows that Santa Anas occur from September to April, with a range of 0.2–3.7 Santa Ana days for these months in 1980–2009. Our results are closest to those of Jones et al. (2010), who diagnosed Santa Ana days by analyzing *SLP* and winds from the NCEP-Department of Energy (DOE) reanalysis.

In Fig. 9 we further refine our definition of Santa Anas by examining the relationships among the daily values for the *SLP* gradient and *RH* as defined above, and the area burned in SW California during autumn. In September, large fires are more likely occur when *RH* is low, but the size of fires does not depend on the *SLP* gradient. In October, the fire size is significantly correlated with the *SLP* gradient ( $r = 0.3$ ) and is inversely correlated with *RH* ( $r = -0.26$ ). Similar results are found for November, but the fires are much smaller than in October because of damper weather. We find that over 75 % of the total area burned in October and 50 % in November occurs on the days when the *SLP* gradient exceeds 10 hPa and the *RH* is less than 25 %, as shown by the dashed lines in Fig. 9. We therefore define strong Santa Anas as those days characterized by  $\Delta SLP$  and *RH* beyond these thresholds. With this definition, we find no strong Santa Ana days in September in 1980–2009, consistent with the absence of large fires in this month during that time frame (Fig. 9a). However, unusually strong Santa Ana winds in late September 1970 resulted in an extremely large ( $1.1 \times 10^5$  ha) wildfire near San Diego ([http://www.wildfirelessons.net/documents/Laguna\\_Fire\\_Analysis\\_1970.pdf](http://www.wildfirelessons.net/documents/Laguna_Fire_Analysis_1970.pdf)). Figure 9 indicates that

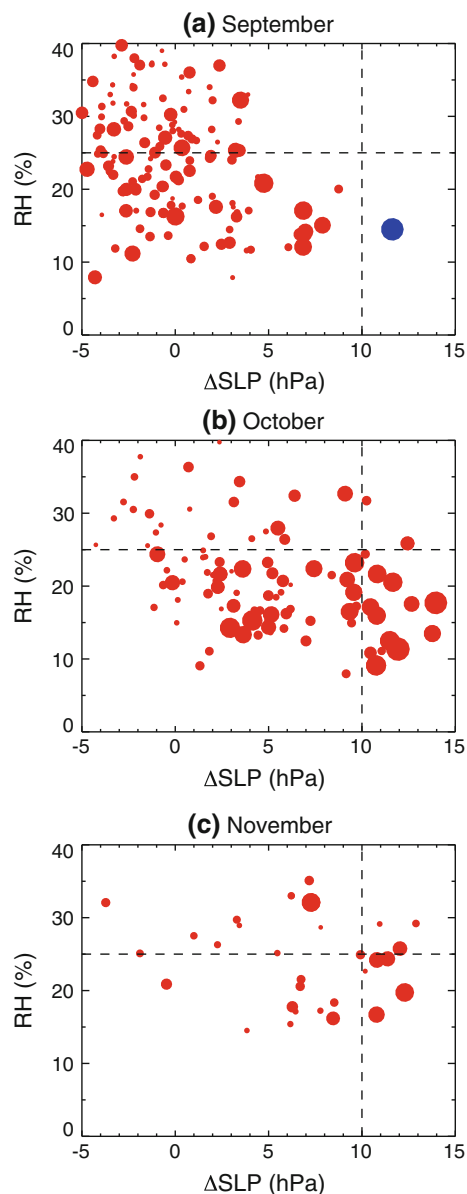


**Fig. 9** Relationships between daily area burned (>10 ha) in southwestern California, sea level pressure gradient between the Great Basin and Los Angeles, and the relative humidity close to San Diego in **a** September, **b** October, and **c** November for the period 1980–2009. The two regions used to define the *SLP* gradient are shown in Fig. 6b, and the region used to define *RH* is shown in Fig. 6e. Positive values of  $\Delta SLP$  mean that *SLP* is greater over the Great Basin than over Los Angeles. Two dashed lines indicate the thresholds for  $RH = 25\%$  and  $\Delta SLP = 10$  hPa. Each red point indicates a fire occurrence, with the symbol size proportional to the logarithmic area burned. The largest point (in October, 2003) represents an area burned of  $\sim 1,100$  km<sup>2</sup>. The blue point in (a) denotes the Laguna fire occurring on September 26th, 1970. Meteorology for this fire alone is from the NCEP reanalysis since the NARR reanalyses date back only to 1979

though Santa Ana events increase the likelihood of large wildfires, some large fires occur in the absence of Santa Anas, a finding also reported by Moritz (1997).

### 3.3.3 Parameterization of area burned

In Y2013, we developed a parameterization for wildfire area burned as follows:

$$\ln(AB) = \begin{cases} \frac{\alpha \cdot T \cdot (1.0 - RH/100)^2}{T_t \cdot (R + 0.2)} & \text{if } T > T_t \text{ and } R < R_t \\ \text{no fire} & \text{otherwise} \end{cases} \quad (4)$$

where  $AB$  is area burned,  $T$  is temperature ( $^{\circ}C$ ),  $R$  is precipitation ( $mm \text{ day}^{-1}$ ), and  $RH$  is RH (%). The threshold values are  $T_t = 15.0 \text{ }^{\circ}C$  and  $R_t = 2.5 \text{ mm day}^{-1}$ . We proposed the above functional form because our analyses showed that the observed  $\ln(AB)$  is linearly correlated with  $T (1 - RH/100)^2$ , and  $(R + 0.2)^{-1}$  in the western U.S. This relationship also depends on the fire potential coefficient  $\alpha$ , which is a function of such factors as ignition, elevation, and fuel load. In Y2013, this coefficient was determined a posteriori, such that the long-term annual mean area burned matched that observed in each ecoregion. Y2013 found that simulations with Eq. (4) using the  $1^{\circ} \times 1^{\circ}$  NARR meteorology captured the seasonality and interannual variability of area burned in most ecoregions in the West, but not for those in southern California.

Here we aggregate the updated area burned and NARR meteorology onto a  $0.5^{\circ} \times 0.5^{\circ}$  grid. We demonstrate that Eq. (4) still works reasonably well for the finer grid cells in southern California (section B in the supplemental information). We also include the relative fire probability in the function by defining  $\alpha = \alpha' \times FP(x, y)$ , where  $\alpha'$  is a scaling factor that forces the predicted mean area burned for 1980–2009 to match the observations in each ecoregion. Finally, we use daily  $SLP$  and  $RH$  from the reanalyses to diagnose strong Santa Ana events in SW California as follows,

$$\ln(AB^*) = \begin{cases} \ln(AB) + 2.3 & \text{if } 1 - \text{day strong Santa Ana} \\ \ln(AB) + 5.3 & \text{if } \geq 2 \text{ days strong Santa Ana} \\ \ln(AB) & \text{otherwise} \end{cases} \quad (5)$$

The value of  $\ln(AB)$  is calculated from Eq. (4). The constants 2.3 and 5.3 are determined empirically so that the simulated area burned matches the observed during strong Santa Anas. In this case, a one-day strong Santa Ana wind increases the predicted area burned by a factor of 10. If the Santa Ana event lasts two days or more, area burned in our model increases by a factor of 200, consistent with the large impact of strong Santa Ana events on wildfire activity as shown in Fig. 9.

Figure 10 compares the simulated area burned with observations. In SW California, the correlation  $r$  between the simulated and observed annual area burned is 0.80 (and 0.92 for October, for which we determined the constants in Eq. 5). The parameterization matches the largest area burned in 2003, but underestimates that in 2007 by  $\sim 50 \%$ . In 2007, there was

a fire in October associated with Santa Ana winds, but the temperatures and precipitation were relatively normal. If we remove these 2 years, the correlation  $r$  drops to 0.59 but is still significant. The simulation underestimates other relatively high fire years, particularly 2006, but also 1996 and 2009, by 50–70 % (Fig. 10a). Area burned was highest in September in 2006 and in August in 2009, indicating that factors other than Santa Ana winds were responsible at those times. For the Sierra Nevada, the parameterization misses many large fire years, but yields a significant correlation ( $r = 0.52$ , Fig. 10e). The parameterization is not successful in CW California (Fig. 10c). Our regression analysis shows that weather conditions in previous years influence area burned in both these regions (Table 2), a factor that the parameterization does not take into account.

The parameterization captures the seasonality of area burned in all three ecoregions, and in particular reproduces the October peak in SW California (Fig. 10). In the other regions, the parameterization captures the seasonality of area burned because it is similar to that of temperature (Fig. 2 and S1). Finally, using sensitivity tests, we demonstrate that the finer spatial resolution and the inclusion of relative fire probability and impacts of Santa Ana winds in the parameterization help improve the predicative capability for area burned in southern California (see section C in the supplemental information).

## 4 Projection of area burned at the midcentury

We apply the CMIP3 archived meteorology from 14 GCMs to both the regression and parameterization models (Table 1). We first validate our approach by examining the results with present-day GCM meteorology. For the projections of area burned in the future, we assume that the fire-weather relationships derived for the present day hold in a future climate. We also do not consider the possible impacts of changing population or fuel load. For the regression models, we aggregate daily gridded data from the GCMs in the three ecoregions. We bias-correct the merged daily output with monthly mean observations for 1980–2009 from FAMWEB sites. Only the long-term means of the GCM output are corrected, not their variance. The bias-corrected daily values are then used to calculate daily CFWIS indexes and to derive the monthly averages that are used as input to the regressions in Table 2. For the parameterization, we bias-correct the GCM output with monthly mean NARR reanalyses in each  $0.5^{\circ} \times 0.5^{\circ}$  grid box. The bias-corrected meteorological fields, including temperature, precipitation,  $RH$ , and  $SLP$ , are used to predict area burned for the present day and at midcentury with Eqs. 4 and 5. Since the parameterization has no predictive capability in CW California, we do not use it there.

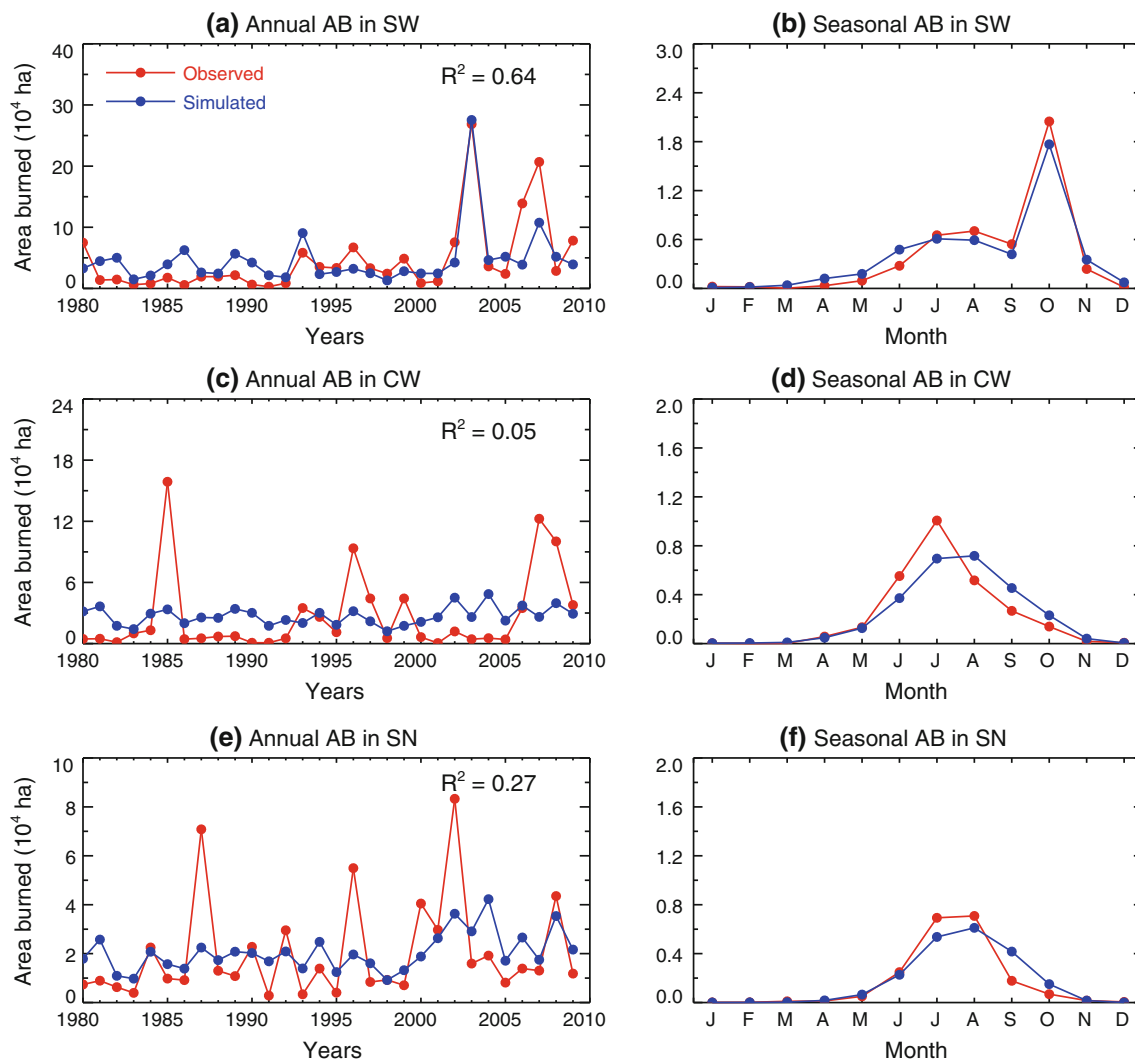


**Fig. 10** Observed (red) and simulated (blue) area burned in three ecoregions of Southern California during 1980–2009. **a**, **c**, and **e** show the time series of total annual area burned; **b**, **d**, and **f** show the average monthly mean values during this time period. In all panels,

the simulated area burned is calculated with the parameterization. The correlation  $r$  between the observed and simulated area burned is significant at  $p < 0.001$  in southwestern California and  $p < 0.005$  in the Sierra Nevada, but is insignificant in central western California

#### 4.1 Evaluation of present-day area burned

We find that seven GCMs predict an October peak in area burned in SW California (Fig. 11), and yield a correlation of  $r > 0.9$  with the observed monthly mean area burned. Six of these GCMs predict area burned in October within a factor of two of that observed, while the seventh significantly underestimates the area. The seven GCMs whose result best match observations predict an average  $RH$  of 15–20 % in the San Diego box area (Fig. 6e) during the Santa Ana days, while the other GCMs predict average  $RH$  of 19–23 %, resulting in fewer (by 27 % on average) strong Santa Ana events. We use these seven best GCMs to compare projections with both regressions and parameterization. We also show results for all 14 GCMs for the regression approach.

We compare annual area burned predicted using GCM output for 1981–2000 to observed (1980–2009) area burned in Fig. 12. For regression models using output from 14 GCMs, the median ratios are 1.36 in SW California, 1.07 in CW California, and 0.95 in the Sierra Nevada (Fig. 12a). Although we bias-correct the meteorological variables with observations, biases in the predictions persist in ecoregions that use CFWIS indexes as regression terms (Table 3). For example, the GCM that gives double the present-day area burned in SW California has the greatest  $DSR_{max}$  among the seven models because it predicts  $\sim 6$  days with high winds ( $>6 \text{ m s}^{-1}$ ) during every fire season, compared with a median of 3.5 days in the other GCMs. The predictions with 7 GCMs (Fig. 12b) shows similar median ratios to those with 14 GCMs

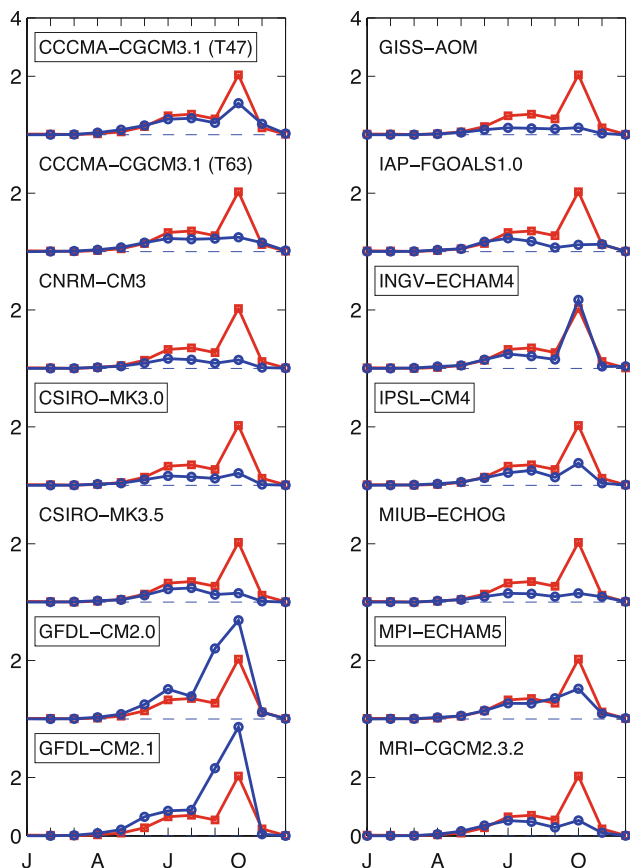


**Fig. 11** Observed (red) and predicted (blue) seasonality of present-day area burned ( $10^4$  ha) in southwestern California by 14 GCMs. Each point represents the monthly mean averaged over 1981–2000 in the 20C3 M scenario. All predictions are calculated using the parameterization. We box the names of the 7 models whose monthly mean area burned correlate with observations with  $r$  greater than 0.9

(Fig. 12a). For predictions with the parameterization, the median ratios of calculated to observed area burned are 0.8–0.9 for SW California and the Sierra Nevada (Fig. 12c). The two GCMs with the highest ratios of 1.7–2.0 predict 2–3 strong Santa Ana days per autumn, typical for this time of year, but also yield 7–8 extremely hot and dry days ( $T > 35$  °C and  $RH < 20$  %) during every fire season, much more than the 1–4 similar days in the other GCMs.

#### 4.2 Prediction of future area burned

##### 4.2.1 Changes in meteorology by mid-century (2046–2065)

Temperatures increase by 0.8–3.8 °C in summer in the 14 GCMs, with median changes 2.0–2.5 °C as shown in Fig. 13a. These increases are significant in all GCMs in each ecoregion. This is not the case for precipitation (already low in summer) and  $RH$ , where the sign of the change is uncertain, with small median changes (Fig. 13b,

c). Only 1–4 models predict significant changes in precipitation and  $RH$ , depending on the ecoregion. For all variables, the median values for the seven GCMs used with the parameterization are similar to those for all 14 GCMs.

Three of seven GCMs predict increases of 0.15–0.25 strong Santa Ana days in September by mid-century relative to present day, as shown in Fig. 14a, with similar results for October but for different GCMs. The other GCMs predict either no change or decreases. However, none of the trends are significant even for  $p < 0.1$ . Changes in the number of strong Santa Ana days are more robust in November, with all GCMs predicting increases of 0.1–0.65 days; changes are significant for four GCMs ( $p < 0.1$ ). Our results are consistent with those of Miller and Schlegel (2006) who found uncertain changes in Santa Anas in September and October but consistent increases in November and December in the late twenty-first century, based on the pressure gradient simulated by two GCMs for two scenarios. Over southwestern California, all seven GCMs predict significant increases in temperature, with a median warming of  $\sim 2.5$  °C in autumn (Fig. 14b). For  $RH$ , 5–6 GCMs predict more moist air in September and October while 5 project drier conditions in November (Fig. 14c). Such changes are not significant except in November for two GCMs.

##### 4.2.2 Changes in area burned

Using the regressions, we find that the median area burned increases in all three ecoregions by mid-century in response to climate change (Fig. 15). The increases are largest in SW California, with a median doubling of area burned whether 7 or 14 GCMs are used; all increases are significant (Fig. 15). For simulations with all 14 GCMs, the median frequency of high fire years (annual area burned  $> 10^5$  ha), increases from 2 to 12 in 2046–2065 (Fig. 16). A similar increase in the high fire years is simulated with the seven selected GCMs. Median increases of area burned are smaller in CW California (10 %) and the Sierra Nevada (35 %) (Fig. 15a), and these increases are significant only for two and seven GCMs, respectively (Fig. 15d). We find similar median changes projected with the seven selected GCMs, except in CW California, where area burned increases by 20 % (Fig. 15b). Only 2 GCMs predict significant increases in the Sierra Nevada (Fig. 15e).

In SW California the increase in temperature drives the increase in area burned (Table 3). The regression model shows little change in  $DSR_{max}$  between mid-century and present day (Table 3), likely because climate models have difficulties in capturing the changes in surface wind speed in complex topography. In the Sierra Nevada, temperature also appears in the dominant regression terms (Table 3). However, the two temperature terms offset each other in

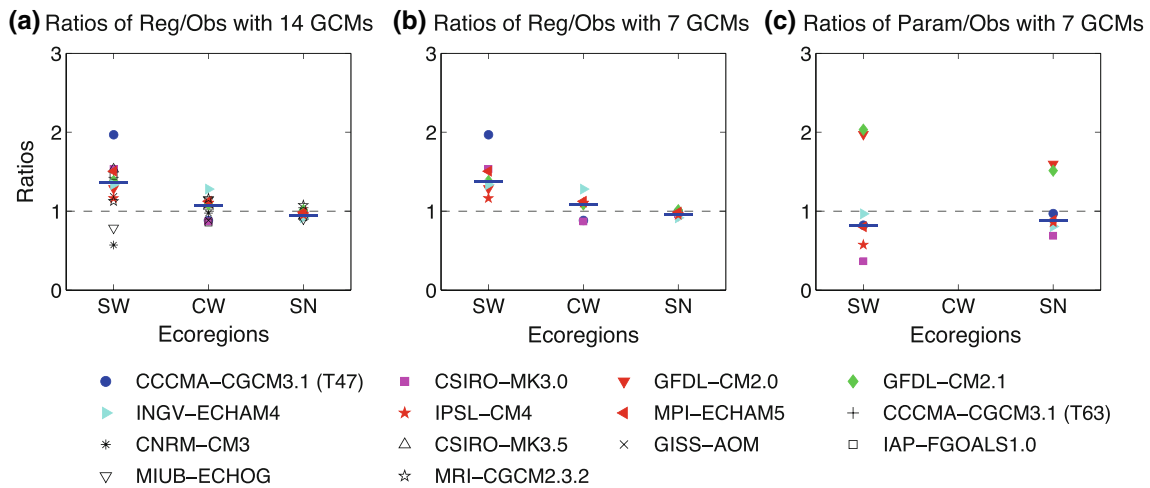


**Fig. 12** Ratios of simulated to observed area burned for the present day with regressions using output from **a** all 14 GCMs and **b** the 7 selected GCMs. **c** Shows the ratios calculated with the parameterization using output from the same 7 GCMs as in **(b)**. Different symbols represent results from different models, and are averages over 1981 to 2000 for the present day. The short bold lines denote the median ratio over each ecoregion. Acronyms for the ecoregions are defined in Fig. 2

**Table 3** Changes in calculated regression terms at midcentury, and their contributions to the changes in area burned predicted by the regression models for the A1B scenario

Ecoregions	Obs Mean 1980–2009	Simulated median		# of models ( $p < 0.05$ ) <sup>a</sup>	Changes in Reg. terms <sup>b</sup>	Percent contribution <sup>c</sup>
		1981–2000	2046–2065			
<b>SW California</b>						
T.FS (°C)	28.7	28.7	31.0	14	$6.9 \times 10^4$	98
DMC <sub>max</sub> (-2)	539.1	590.2	578.6	2	$-0.1 \times 10^4$	2
DSR <sub>max</sub>	58.3	72.3	72.6	1	0	0
<b>CW California</b>						
RH.ANN (%)	43.2	42.7	42.1	2	$3.5 \times 10^3$	81
DC(-2)	841.7	862.9	868.0	0	$-0.8 \times 10^3$	19
<b>Sierra Nevada</b>						
T <sub>max</sub> .AUT(-2) (°C)	21.0	21.1	25.3	14	$-2.6 \times 10^4$	44
T.FS (°C)	24.1	24.0	27.9	14	$3.3 \times 10^4$	56

Definitions of the regression terms are provided in Table 2

<sup>a</sup> Number out of 14 models that predict significant changes in meteorological variables in each ecoregion, as determined by a one-tailed Student’s *t* test. If the median value of the change is positive, only those predicting a significant increase are counted and vice versa for a negative change

<sup>b</sup> Shown are the changes in variables multiplied by the regression coefficients for the median model in each ecoregion. Here we define the median model as that model which predicts the 7th maximum ratio of future to present-day area burned out of all 14 GCMs in each ecoregion (Fig. 15a)

<sup>c</sup> Percent contributions of the absolute changes in individual regression terms to the sum of changes for the median model in each ecoregion

the regression (Table 2), resulting in small insignificant changes in area burned (Fig. 15e) in this region. In CW California, changes in RH contribute more than those in the drought code index; the small changes predicted in hydrological variables lead to large uncertainty in future fire activity.

The uncertainty in the projections of future area burned is indicated by the spread of the symbols in Fig. 15a. The largest

spread is in SW California, with 6 of 14 models projecting ratios of future to present-day area burned outside the  $\pm 20\%$  range of the median ratio. The large spread follows that in temperature (Fig. 13a). Two GCMs predict more than tripling of area burned in this ecoregion, due to the anomalously low area burned predicted by these two GCMs in the present day (Fig. 12a). The smallest spread of projections is for the Sierra Nevada, where the ratios from 13 GCMs are within  $\pm 20\%$  of

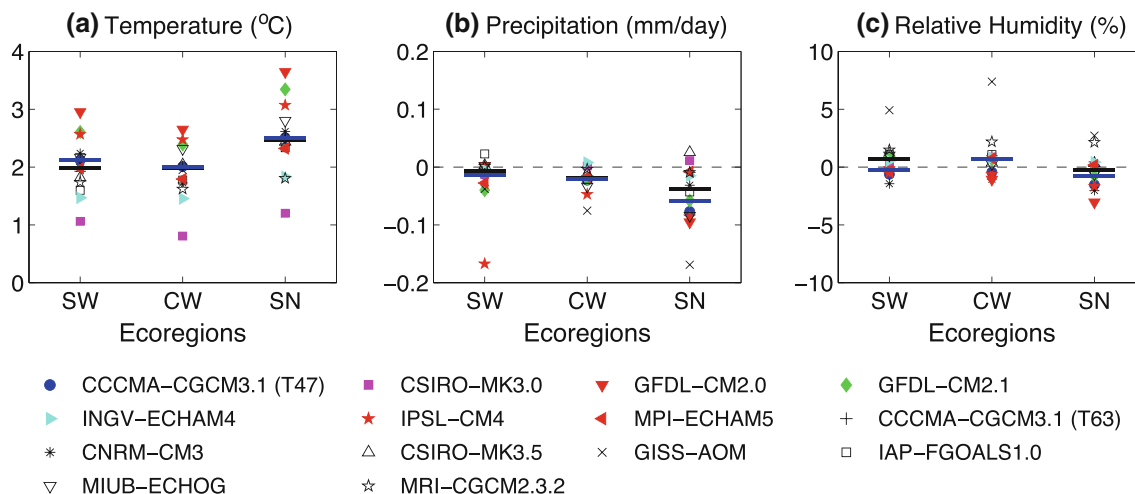


**Fig. 13** Predicted changes in **a** temperature, **b** precipitation, and **c** relative humidity over three ecoregions in Southern California in the boreal summer by midcentury for 14 climate models in the A1B scenario, relative to the present day. Different symbols represent results from different models. The **dark bold lines** denote the median

values from all 14 GCMs. The **blue lines** are the medians from the seven GCMs which best represent Santa Ana events in southwestern California (Sect. 4.1 of text). Acronyms for the ecoregions are defined in Fig. 2

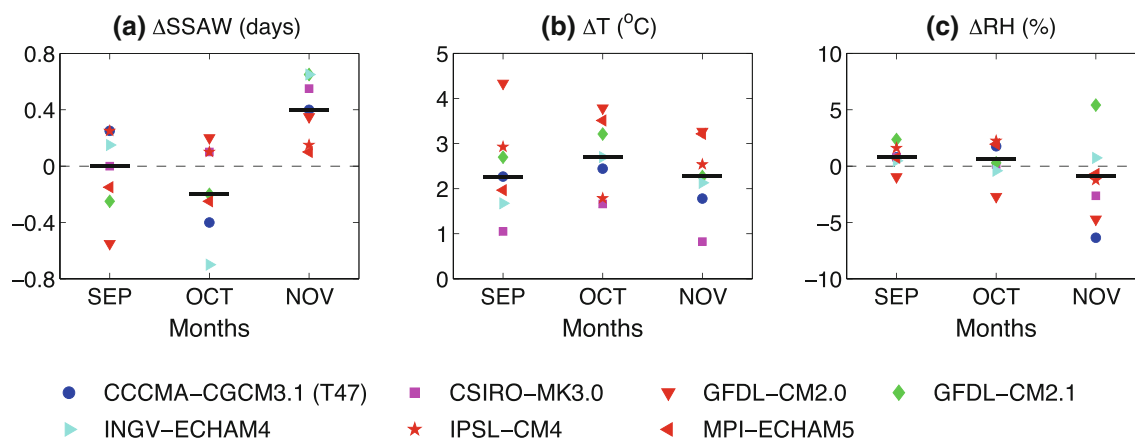


**Fig. 14** Predicted changes in **a** strong Santa Ana days, **b** temperature, and **c** relative humidity for three autumn months in Southwestern California by midcentury, relative to the present day. Results are shown for only the seven selected climate models which best

represent Santa Ana events. *Different symbols* denote results from different models. The **black bold lines** are the median changes from the seven GCMs

the median. All climate models except one project ratios close to 1.0 in CW California, and the exception predicts significant increases in the local relative humidity at midcentury (Fig. 13c). The uncertainty is smaller for projections with the seven selected GCMs (Fig. 15b), because some extreme ratios are excluded.

Using the parameterization approach, the median area burned increases by 40 % in SW California (Fig. 15c). However, this increase is significant for only two of the seven GCMs, those that predict the highest increases in the number of strong Santa Ana days in autumn (30 and 40 %, Fig. 14a). In contrast, one model predicts a decrease of 60 % in the number of strong Santa Ana days in October, resulting in decreases of area burned by 85 % in the same month (Fig. 17) and by 20 %

in the annual total (Fig. 15c). Because of the large variability of modeled Santa Ana activity, none of the GCMs predict significant changes in the number of strong Santa Ana days by midcentury. As a result, the median frequency of extreme fire years (annual area burned >10<sup>5</sup> ha) is at a level of once in 20 years for both present-day and future (Fig. 16). We find that the spread of the predictions of area burned in this region is related to that in the prediction of strong Santa Anas, especially in October (Fig. 14a). For the Sierra Nevada, six GCMs predict significant increases in area burned (Fig. 15f), resulting in a median change of ~50 % (Fig. 15c).

The parameterization gives predictions of monthly area burned in addition to annual area burned. All seven GCMs predict increases in area burned in summer in SW

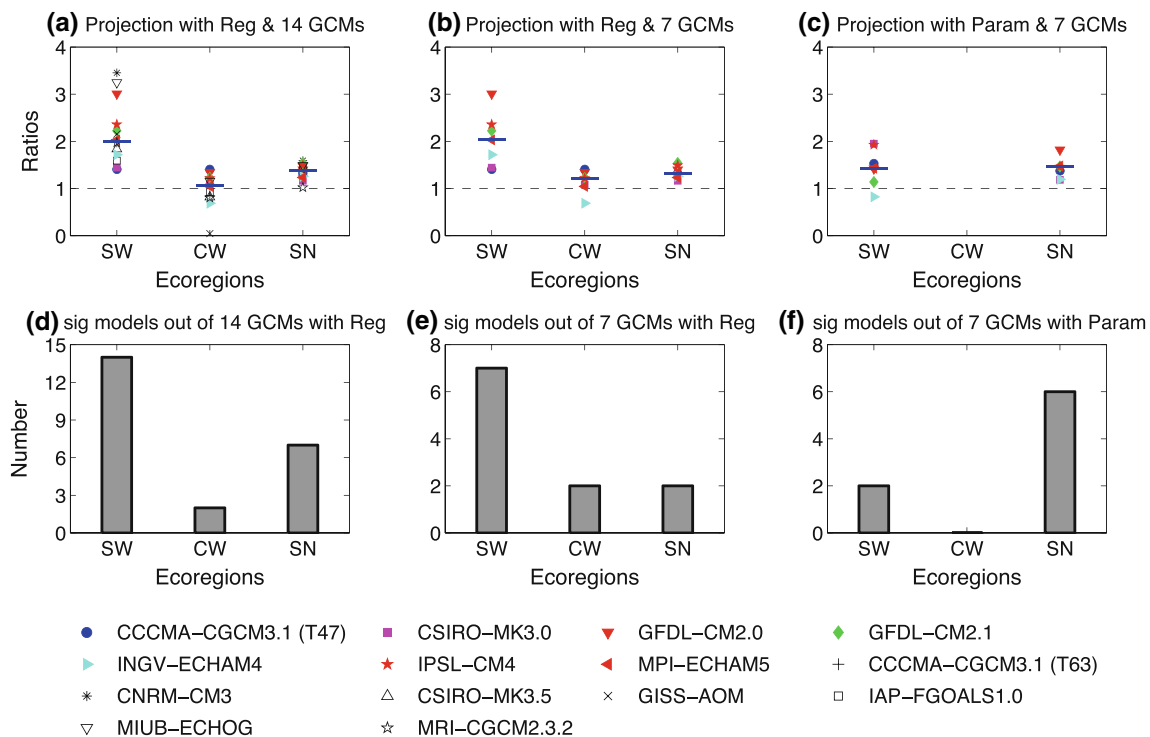


**Fig. 15** Predicted ratio of future area burned to present day area burned in three southern California ecoregions with regressions using output from **a** all 14 GCMs and **b** the 7 selected GCMs. **c** shows the ratios calculated with the parameterization using output from the same 7 GCMs as that in (**b**). The *bottom panels* show the number out of **d** 14 or **e**, **f** 7 GCMs that predict significant changes with the same

sign as the medians. *Different symbols* represent results from different models, and are averages over 1981–2000 for the present-day and 2046–2065 for the future. The *short bold lines* denote the median ratio over each ecoregion. Acronyms for the ecoregions are defined in Fig. 2

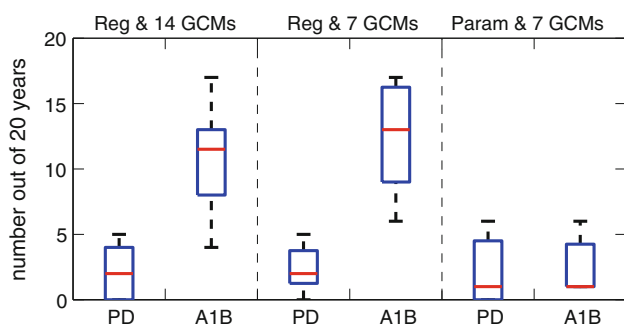


**Fig. 16** Prediction of number of years with annual area burned  $>10^5$  ha out of the twenty-year period for SW California in present day and midcentury. The panels represent results calculated with (*left*) regressions using output from 14 GCMs, (*middle*) regressions using output from 7 GCMs, and (*right*) the parameterization using output from 7 GCMs. The predictions for present day (1981–2000) are shown in the *left column* for each panel, while those for midcentury (2046–2065) are shown in the *right column*. The *blue box* shows the interquartile range of model predictions. The *red lines* within the *box* indicate the medians. The annual area burned does not exceed  $10^5$  ha for the other two southern California ecoregions with either approach

California (Fig. 17). Five predict increases in autumn as well, and these changes are 2.5–5 times those in summer for four of them. Four GCMs predict larger area burned in September, while two of these four and two others also

predict increases in October, the peak fire month in 1980–2009 (Fig. 17). In three GCMs, the peak fire month shifts to September due to changes in the activity of strong Santa Ana events (Fig. 14a), but these changes are not significant even at  $p < 0.1$ .

A more robust finding is that future wildfire activity in SW California may extend to November. In the present-day atmosphere, more Santa Ana days occur in November than in October (Fig. 8), but the cool and wet weather in November inhibits the spread of fires. By midcentury, the GCMs predict that the frequency of strong Santa Ana events increases by  $\sim 0.4$  days (130 %) in November (Fig. 14a). The warmer and drier autumn climate, in turn, leads to a median increase of 360 % in the average fire area on each strong Santa Ana day in this month. Taken together, these factors lead to an increase in the area burned in November by factors of 2.4–7.6 by midcentury, which is significant at the  $p < 0.1$  level for four GCMs.

## 5 Discussion and conclusions

We predicted future area burned by wildfires in three ecoregions of southern California in midcentury with two



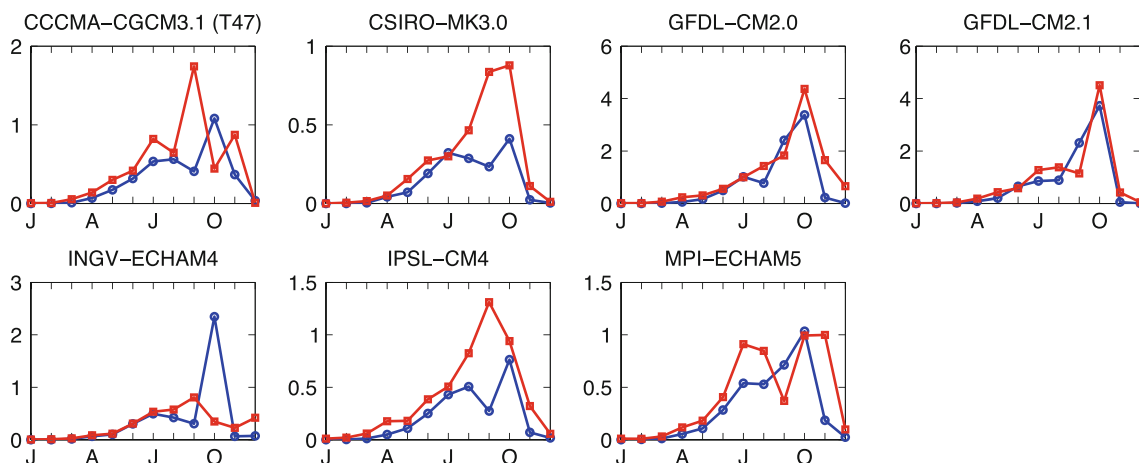


**Fig. 17** Predicted seasonality of area burned ( $10^4$  ha) in the present day (blue) and at midcentury (red) in southwestern California by the seven selected GCMs which best capture Santa Ana events. Each

point represents the total area burned in each month, averaged over 1981–2000 for present day and 2046–2065 for midcentury

fire prediction schemes and output from multiple CMIP3 GCMs. The regressions, which take into account the impacts of current and antecedent meteorological variables and fire indexes, capture 40–46 % of the variance of observed area burned in three ecoregions during 1980–2009. The parameterization includes the dependence of area burned on temperature, *RH*, and precipitation, together with the influence of topography, population, and fuel load on local fire probability. We also parameterized the impact of the Santa Ana, a strong offshore and dry wind that is responsible for many extremely large fires in autumn in southern California (Keeley et al. 2009). With these improvements, the parameterization explains 64 % of the variance in observed annual area burned in SW California and reproduces its seasonality reasonably well. It also captures 27 % of the variance of area burned in the Sierra Nevada. For all of southern California, the relationships for the three sub-regions developed here give  $R^2$  of 0.59 for the regressions and 0.38 for the parameterization. Our results represent a major improvement over those in Y2013 for California coastal shrubland, where our previous models showed little or no predictive capability.

Using meteorology from the CMIP3 ensemble of 14 GCMs, the regressions project that median area burned will double in SW California and increase by 35 % in the Sierra Nevada and by 10 % in CW California by midcentury. The spread of the predictions is largest in SW California, following the spread of temperature change. However, increasing temperature is a robust result of all models for this ecoregion, and drives the statistically significant increases in area burned. Extreme fire years (annual area burned  $> 10^5$  ha) increase in SW California from one per decade in the present day to 6–7 per decade at midcentury.

In contrast, only half the GCMs predict significant increases in future area burned in the Sierra Nevada and only two do so in CW California, either due to little change in the *RH* or the offset between two competing temperature factors.

For the projection with parameterization, we focused on output from the seven GCMs that successfully capture the observed seasonality of area burned in SW California. With these models, the median area burned is projected to increase by 40 % in SW California and 50 % in the Sierra Nevada by midcentury. For the Sierra Nevada, six GCMs predict significant increases in annual area burned. For SW California, the only GCMs that predict significant increases are the two that show increases in Santa Ana days of 30 % or more by midcentury. For this ecoregion, however, all seven GCMs predict increases in area burned (140–660 %) in November because of the combination of a greater frequency of Santa Ana events and the warmer and drier fire weather.

Taken together, these results suggest that wildfire activity is likely to increase in SW California and the Sierra Nevada in coming decades as a consequence of rising surface temperatures. In SW California, the regressions predict that area burned could double by midcentury, while the parameterization projects a significantly longer fire season extending into November. Our use of multiple GCMs and two fire schemes allows us to make these predictions with greater confidence than earlier studies. Individual GCMs can yield quite different trends, as seen previously (e.g., Westerling and Bryant 2008; Lenihan et al. 2008; Westerling et al. 2011). In our study, however, the median values of the large ensemble of 14 GCMs provide some certainty in our estimates for future area

burned. Our study is also the first to consider the effect of the Santa Anas, an important driver for the observed interannual variability of local area burned in SW California. Our definition of strong Santa Anas allows diagnosis of these events even in coarse-grid GCMs. We find that the increase in modeled Santa Anas in November at mid-century contributes to the significant enhancement in area burned at that time of year.

Our approach does not consider climate-induced changes in fuel load (Lenihan et al. 2008) or changes in population (Safford 2007), both of which may influence the fire frequency and regime (Syphard et al. 2007; Peterson et al. 2011). We also did not consider trends in human activity which may influence wildfires, a factor included in Westerling et al. (2011). Finally, we were unable to diagnose a significant trend in wildfire activity in CW California. Few GCMs in our ensemble simulate significant changes in the hydrological variables in the 2050 s atmosphere in California, and the large inter-model spread makes even the sign of these changes uncertain (Fig. 13). Such uncertainties result in low confidence in the projection of area burned in CW California, where hydrological factors dominate the fire-weather relationship.

A longer and more intense fire season in the 2050 s atmosphere would threaten the safety of California residents and increase the expense of fire suppression, which currently amounts to about one billion dollars annually (Safford 2007). An expansion of fire area would increase biomass burning emissions, seriously degrading both air quality and visibility locally and downwind (Hlavka et al. 2005; Pfister et al. 2008). Increased exposure to smoke would endanger human health and add to the economic cost of fires (Kunzli et al. 2006; Hanninen et al. 2009; Richardson et al. 2012). Quantification of these air quality and health effects requires confidence in the projections of future area burned, such as our multi-model study provides.

**Acknowledgments** We would like to thank Zhiming Kuang and Brian F. Farrell for useful advice in diagnosing Santa Anas in GCMs. We are grateful for the helpful discussion with Dr. Yufang Jin at University of California, Irvine. We acknowledge the modeling groups, the Program for Climate Model Diagnosis and Intercomparison (PCMDI) and the WCRP's Working Group on Coupled Modelling (WGCM), for making available the WCRP CMIP3 multi-model dataset. Support of this dataset is provided by the Office of Science, U.S. Department of Energy. This work was funded by STAR Research Assistance agreement R834282 awarded by the U.S. Environmental Protection Agency (EPA). Although the research described in this article has been funded wholly or in part by the EPA, it has not been subjected to the Agency's required peer and policy review and therefore does not necessarily reflect the views of the Agency and no official endorsement should be inferred. Research reported in this publication was supported in part by the NASA Air Quality Applied Science Team and the National Institutes of Health (NIH) under Award Numbers 1R21ES021427 and 5R21ES020194. The content is solely the responsibility of the authors and does not necessarily represent the official views of the NIH.

## References

- Abatzoglou JT, Barbero R, Nauslar NJ (2013) Diagnosing Santa Ana winds in southern California with synoptic-scale analysis. *Weather Forecast* 28:704–710
- Christensen JH, Hewitson B, Busuioc A, Chen A, Gao X, Held I, Jones R, Kolli RK, Kwon W-T, Laprise R, Rueda VMA, Mearns L, Menéndez CG, Räisänen J, Rinke A, Sarr A, Whetton P (2007) Regional Climate Projections. In: Solomon S, Qin D, Manning M, Chen Z, Marquis M, Averyt KB, Tignor M, Miller HL (eds) *Climate change 2007: working group I: the physical science basis*. Cambridge University Press, Cambridge
- Conil S, Hall A (2006) Local regimes of atmospheric variability: A case study of southern California. *J Clim* 19:4308–4325
- Flannigan MD, Logan KA, Amiro BD, Skinner WR, Stocks BJ (2005) Future area burned in Canada. *Clim Change* 72:1–16
- Hanninen OO, Salonen RO, Koistinen K, Lanki T, Barregard L, Jantunen M (2009) Population exposure to fine particles and estimated excess mortality in Finland from an East European wildfire episode. *J Expo Sci Environ Epidemiol* 19:414–422
- Hickman J (1993) *The Jepson manual: higher plants of California*. University of California Press, Berkeley
- Hlavka DL, Palm SP, Hart WD, Spinhirne JD, McGill MJ, Welton EJ (2005) Aerosol and cloud optical depth from GLAS: results and verification for an October 2003 California fire smoke case. *Geophys Res Lett* 32:L22S07. doi:10.1029/2005GL023413
- Hughes M, Hall A (2010) Local and synoptic mechanisms causing Southern California's Santa Ana winds. *Clim Dyn* 34:847–857
- Hughes M, Hall A, Kim J (2011) Human-induced changes in wind, temperature and relative humidity during Santa Ana events. *Clim Change* 109:119–132
- Jones C, Fujioka F, Carvalho LMV (2010) Forecast skill of synoptic conditions associated with Santa Ana winds in southern California. *Mon Weather Rev* 138:4528–4541
- Keeley JE, Safford H, Fotheringham CJ, Franklin J, Moritz M (2009) The 2007 southern California wildfires: lessons in complexity. *J For* 107:287–296
- Kunzli N, Avol E, Wu J, Gauderman WJ, Rappaport E, Millstein J, Bennion J, McConnell R, Gilliland FD, Berhane K, Lurmann F, Winer A, Peters JM (2006) Health effects of the 2003 southern California wildfires on children. *Am J Respir Crit Care Med* 174:1221–1228
- Lenihan JM, Bachelet D, Neilson RP, Drapek R (2008) Response of vegetation distribution, ecosystem productivity, and fire to climate change scenarios for California. *Clim Change* 87:S215–S230
- Littell JS, McKenzie D, Peterson DL, Westerling AL (2009) Climate and wildfire area burned in western U. S. ecoregions, 1916–2003. *Ecol Appl* 19:1003–1021
- McKenzie D, Raymond CL, Kellogg LKB, Norheim RA, Andreu AG, Bayard AC, Kopper KE, Elman E (2007) Mapping fuels at multiple scales: landscape application of the Fuel Characteristic Classification System. *Can J For Res* 37:2421–2437
- Meehl GA, Covey C, Delworth T, Latif M, McAvaney B, Mitchell JFB, Stouffer RJ, Taylor KE (2007) The WCRP CMIP3 multi-model dataset: a new era in climate change research. *Bull Am Meteorol Soc* 88:1383–1394
- Mesinger F, DiMego G, Kalnay E, Mitchell K, Shafran PC, Ebisuzaki W, Jovic D, Woollen J, Rogers E, Berbery EH, Ek MB, Fan Y, Grumbine R, Higgins W, Li H, Lin Y, Manikin G, Parrish D, Shi W (2006) North American regional reanalysis. *Bull Am Meteorol Soc* 87:343–360
- Miller NL, Schlegel NJ (2006) Climate change projected fire weather sensitivity: California Santa Ana wind occurrence. *Geophys Res Lett* 33:L15711. doi:10.1029/2006gl025808

- Moritz MA (1997) Analyzing extreme disturbance events: fire in Los Padres National Forest. *Ecol Appl* 7:1252–1262
- Mott JA, Meyer P, Mannino D, Redd SC, Smith EM, Gotway-Crawford C, Chase E (2002) Wildland forest fire smoke: health effects and intervention evaluation, Hoopa, California, 1999. *Western J Med* 176:157–162
- Ottmar RD, Sandberg DV, Riccardi CL, Prichard SJ (2007) An overview of the Fuel Characteristic Classification System—Quantifying, classifying, and creating fuelbeds for resource planning. *Can J For Res* 37:2383–2393
- Peterson SH, Moritz MA, Morais ME, Dennison PE, Carlson JM (2011) Modelling long-term fire regimes of southern California shrublands. *Int J Wildland Fire* 20:1–16
- Pfister GG, Wiedinmyer C, Emmons LK (2008) Impacts of the fall 2007 California wildfires on surface ozone: Integrating local observations with global model simulations. *Geophys Res Lett* 35:L19814. doi:10.1029/2008gl034747
- Preisler HK, Westerling AL, Gebert KM, Munoz-Arriola F, Holmes T (2011) Spatially explicit forecasts of large wildland fire probability and suppression costs for California. *Int J Wildland Fire* 20:508–517
- Raphael MN (2003) The Santa Ana Winds of California. *Earth Interactions* 7:1–13
- Richardson LA, Champ PA, Loomis JB (2012) The hidden cost of wildfires: economic valuation of health effects of wildfire smoke exposure in Southern California. *J For Econ* 18:14–35
- Safford HD (2007) Man and fire in Southern California: doing the math. *Fremontia* 35:25–29
- Schoennagel T, Veblen TT, Romme WH (2004) The interaction of fire, fuels, and climate across Rocky Mountain forests. *Bioscience* 54:661–676
- Schroeder M, Glovinsky M, Hendricks V, Hood F, Hull M, Jacobson H, Kirkpatrick R, Krueger D, Mallory L, Oertel A, Reese R, Sergius L, Syverson C (1964) Synoptic weather types associated with critical fire weather. Pacific Southwest Forest and Range Experiment Station, Berkeley, CA
- Solomon S, Qin D, Manning M, Chen Z, Marquis M, Averyt KB, Tignor M, Miller HL (2007) *Climate Change 2007: Working Group I: The Physical Science Basis*. Cambridge University Press, Cambridge
- Spracklen DV, Mickley LJ, Logan JA, Hudman RC, Yevich R, Flannigan MD, Westerling AL (2009) Impacts of climate change from 2000 to 2050 on wildfire activity and carbonaceous aerosol concentrations in the western United States. *J Geophys Res* 114:D20301. doi:10.1029/2008jd010966
- Syphard AD, Radeloff VC, Keeley JE, Hawbaker TJ, Clayton MK, Stewart SI, Hammer RB (2007) Human influence on California fire regimes. *Eco Appl* 17:1388–1402
- Syphard AD, Radeloff VC, Keuler NS, Taylor RS, Hawbaker TJ, Stewart SI, Clayton MK (2008) Predicting spatial patterns of fire on a southern California landscape. *Int J Wildland Fire* 17:602–613
- Van Wagner CE (1987) The development and structure of the Canadian forest fire weather index system. Canadian forest service, forest technical report 35, Ottawa, Canada
- Westerling AL, Bryant BP (2008) Climate change and wildfire in California. *Clim Change* 87:S231–S249
- Westerling AL, Gershunov A, Brown TJ, Cayan DR, Dettinger MD (2003) Climate and wildfire in the western United States. *Bull Am Meteorol Soc* 84:595–604
- Westerling AL, Cayan DR, Brown TJ, Hall BL, Riddle LG (2004) Climate, Santa Ana winds and autumn wildfires in Southern California. *EOS* 85:289–296
- Westerling AL, Bryant BP, Preisler HK, Holmes TP, Hidalgo HG, Das T, Shrestha SR (2011) Climate change and growth scenarios for California wildfire. *Clim Change* 109:445–463
- Wu WR, Dickinson RE (2004) Time scales of layered soil moisture memory in the context of land-atmosphere interaction. *J Clim* 17:2752–2764
- Yue X, Mickley LJ, Logan JA, Kaplan JO (2013) Ensemble projections of wildfire activity and carbonaceous aerosol concentrations over the western United States in the mid-21st century. *Atmos Environ* 77:767–780